MICELLAR SHAPES AND SOLUBILIZATION PROPERTIES OF DETERGENT SOLUTIONS

*Ji-Sun Kim, Chang-Kew Kim, and *Pill-Soon Song*

Pacific Chemical Co., Ltd., Research and Development Laboratory, Dongjak-Ku, Shindaebang-Dong #656-9 Seoul, Korea.
**Department of Chemistry, Texas Tech University, Lubbock, TX79409, U.S.A.*

I. SUMMARY

The fluorescence intensity ratios (F_2/F_1) of excimer (F_2) to monomer (F_1) of pyrene were measured as a function of the concentration of sodium dodecyl sulfate (SDS). It was found that there were not gross changes in size and shape of sphere-shaped micelles in the first micelle concentration, while at concentrations above the second critical micelle concentration (CMC) the micelles grew in size with increasing concentration. Fluorescence intensities of 8-anilinonaphthalene l-sulfonate (ANS) were also monitored as a micellar probe with varying concentrations of SDS. Results suggested that a phase transition from sphere-shaped micelles to hemicapped rod-like micelles occurred at the second CMC (17). A general formula for the axial ratio of ellipsoid-shaped micelle in the first micelle concentration was suggested. According to this general formula, the axial ratio of SDS, sodium lauryl ether sulfate and sodium laurate were 1:1, 5:2, and 5:3, respectively. The electrolyte-induced phase transition from spherical to hemicapped rod-like micelles occurred and the size of hemicapped rod-like micelles grew with increasing electrolyte concentrations. The maximum concentrations of solubilized benzene in sphere-shaped micelles and hemicapped rod-like micelles were measured by differential spectrophotometry. The hemicapped rod-like micelles in the presence of electrolytes grew in size with increasing amount of benzene solubilized.

II. INTRODUCTION

On of the main reasons for the wide usage of detergents in science and technology is due to their solubilization property. As solubilization power of detergent solutions depends largely on their mecellar shapes, micellar shapes have been studied by many workers.

Although the shape of several micelle systems is well elucidated, particularly at low concentrations near the first critical micelle concentration (CMC) (1,2), there is little definitive information on the shape in the second micelle concentration, where interaction and association among micelles become prominent and interpretations of hydrodynamic to elucidate the topography

of micelles have been performed. For example, studies of electrical anisotropy of micelles (3) suggested that aqueous solutions of cetyl trimethyl ammonium bromide were isotropic in the first micelle concentration, but they were anisotropic in the second micelle concentration. It was also proposed that a phase transition from the spherically shaped to rod-like micelles occurred at the second CMC, as the latter is anisotropic in shape.

Light scattering studies also suggested that the axial ratio of micelles at concentrations above the second CMC increased, with the appearance of rod-like micelles at the second CMC (4). Unfortunately, results from light scattering methods are not interpretable in a straightforward way, and not surprisingly there are many discrepancies in the literature (4-6). A small angle X-ray scattering study yielded no definitive model of micelle in the second micelle concentration, although it suggested that the shape of micelles in the second micelle concentration was different from the spherical shape (7).

In addition, studies by viscosity (4), surface tension (8), conductivity (9), density (9), and NMR, all produced informative data, but none has provided a satisfactory insight into the phase transition at the second CMC. The purpose of this paper is to attempt at elucidating the micellar shape in the first and second micelle concentration range and the relation between micellar shape and solubilization property by means of fluorescence probes. In this work, we use pyrene and 8-anilionaphthalene 1-sulfonate as the fluorescence probe. Results of these fluorescence probe studies are described herein.

III. MATERIALS

Sodium dodecyl sulfate (SDS, Wako) was recrystalized from ethanol. Pyrene (Merck), ammonium 8-anilinonaphthalene 1-sulfonate (ANS, Sigma), 9-methyl anthracene (Merck-Schuchardt), sodium lauryl ether sulfate (SLES, Taedong) and benzene (Wako) were used as received. $Ru(BiPy)_3Cl_3$ was synthesized from ruthenium trichloride (J&J Materials, Inc.) and bipyridine (Merck). Sodium laurate was synthesized from lauric acid (Wako). Deionized water was redistilled twice in the presence of $KMnO_4$.

IV. APPARATUS AND MEASUREMENTS

Fluorescence spectra were recorded on an Aminco-Bowman Spectrofluorometer and were manually corrected point-by-point for the spectral response of the RCA IP21 PM-tube. Corrections for different optical densities of micelle solutions were also performed by multiplying the factor, $1\text{-}10^{-O.D.}$, to each fluorescence intensity, where O.D. is the optical density. Mean aggregation numbers of micelles were determined by the method of Turro and Yetka (10).

Maximum additive concentrations of benzene in SDS solution were determined by differential spectrophotometry as follows: Small amounts (within solubility in water) of benzene were added to ten separate bottles, each con-

taining 50ml of water. After complete sealing, these bottles were shaken for 40 minutes and were then equilibrated at 25°C for 3 days. From absorbance measurements for each solution at 266nm, we obtained the mean molar absorptivity.

An excess amount of benzene (2ml) was added to each 50ml SDS solution containing electrolytes. Solutions were equilibrated. The absorbance differences were then recorded on an Unicam spectrophotometer. The reference cell contained water saturated with benzene. The amount of solubilized benzene for each SDS solution was calculated from the Lambert-Beer Law (O.D. = ECL). The solubility of benzene in water in this experiment was found to be 24.0mM.

V. RESULTS AND DISCUSSION

The relatively long lifetime of the excited singlet state of pyrene and its strong affinity for hydrophobic interactions make pyrene an ideal fluorescence probe for the hydrophobic regions of micelles. Furthermore, the excited pyrene forms a face-to-face excimer with another pyrene in the ground state, thus producing the excimer emission (F_2) at 470nm as well as the monomer emission (F_1) at 390nm (11). As the excimer formation occurs at a diffusion controlled rate (12), the values of F_2/F_1 provide information on the microenvironment of the micellar core area.

Figure 1 shows a plot of F_2/F_1 as a function of SDS concentration. At a fixed pyrene concentration of 0.5mM, the population density of pyrene in micelles decreases with increasing SDS concentrations. As can be seen from Figure 1, a break point occurs at 73mM corresponding to the second CMC of SDS (13). The occurrence of a break point is indicative of a change in micellar shape and/or size at the second CMC.

Figure 2 exhibits the plot of F_2/F_1 as function of SDS concentration, keeping the ratio [pyrene] / [SDS] constant at 1/100. At a constant population density of pyrene in micelles, the values of F_2/F_1 as a function of SDS concentrations directly reflect variations in the microviscosity of micelles. As can be seen in Figure 2, the F_2/F_1 values are constant between 40mM and 70mM SDS, again confirming the results shown in Figure 1 that there are no major changes in the microenvironment of pyrene in the first micelle concentration range.

As the excimer of pyrene is formed via diffusion and face-to-face encounter between the excited and ground state pyrene molecules, the value of F_2/F_1 should depend on the micellar structure. Thus, it is less favorable for the molecules of pyrene to take the face-to-face orientation in spherical micelles then in rod-like micelles. The increasing trend of F_2/F_1 above 70mM, the second CMC of SDS, suggests that the micelles grow to be more like rod-shaped micelles, with increasing SDS concentrations.

Figure 3 displays the plot of mean aggregation number (n) as a function of SDS concentrations above the second CMC. The aggregation number of

micelles at 70mM SDS was found to be $\bar{n} = 54$, in agreement with the previous value, $n = 55 \pm 5$ (14). The linearly increasing tendency of $\bar{n}$ vs. increasing SDS concentrations implies that the total number of micelles above the second CMC is constant. From these observations, we can conclude that the micellar size and shape are probably constant throughout the first micelle concentration ranges and that only teh total number of micelles increases with increasing SDS concentrations. Above the second CMC, the micellar size grows without concomitant increase in the total micellar number with increasing SDS concentrations.

Figure 4 shows the plot of relative fluorescene intensities of ANS (0.32mM) as a function of SDS concentrations. Sharp breakds occur at 8 and 70mM, corresponding to the first (15) and second CMC of the aqueous SDS solution at 25°C, respectively. At the first CMC, micelles begin to form. ANS is soluble in water and its fluorescence is quenched in water below the first CMC. However above the first CMC, ANS molecules are presumably adsorbed at the interface of formed micelles, and their fluorescence emission increases rapidly because of the hydrophobic micellar interface and higher viscosity at the interface than in water. The hydrophobic (napthyl) and hydrophilic (sulfonate) groups of the ANS molecule adsorbed at the interface are probably partitioned into the hydrophobic phase of micelle and the aqueous phase, respectively. Electrostatic interactions between the negatively charged sulfonate and sulface groups of ANS and SDS at the interface. On the bais of results shown in Figure 4 and above considerations, it is suggested that the quantity of ANS adsorbed at the micellar interface is proportional to the total surface area of one micelles in solution and the intensity of ANS fluorescence is proportional to the concentration of ANS adsorbed. Thus, we can write the following equation:

$$I = k \cdot S$$

$$dI/dC = k \cdot dS/dm \qquad [1]$$

where I : fluorescence intensity,
C : total concentration
S : total surface area of micelles,
m : total mass of micelles, and
k : proportionality constant.

The shape of the SDS micelles in the first micells concentration is spherical (2). Thus, we propose that a phase transition from spherically shaped micelles to hemicapped rod-like micelles (5) occurs at the second CMC (cf. Figure 5).

However, diameters of the spherical and circularly curved ends of the hemicapped micelles (cf. Figure 5) are approximately equal.

In the first micelle concentration range, we write

$$S_1 = 4\pi r^2 n_1$$

$$m = \frac{4}{3} \pi r^3 \rho n_1$$

where r : radius of micelle,
ρ : density of micelle, and
n : total micelle number.

At constant r, we have

$$(dS_1/dm)r = 3/r\rho \qquad [2]$$

Simiarly, in the second micelle concentration range, we write

$$S_2 = (4\pi r^2 + 2\pi r1)n_2$$

$$m = \left(\frac{4}{3}\pi r^3 + \pi r^2 1\right)\rho \cdot n_2$$

where 1 is the length of the rod-like micelle (Fig. 5).

At constant r (1 variable), we have

$$(dS_2/dm)\, n_2, r = 2/r\rho \qquad [3]$$

From Eq. (2) and (3), we have

$$\frac{(dS_1/dm)r}{(dS_2/dm)n_2, r} = 1.5 \qquad [4]$$

From Eq. [1], we have

$$\frac{(dS_1/dm)r}{(dS_2/dm)n_2, r} = \frac{dI_1/dC}{dI_2/dC} \qquad [5]$$

From Figure 4

$$\frac{dI_1/dC}{dI_2/dC} = 1.51 \qquad [6]$$

The value of 1.5 in Eq. [4] is the theoretical value for the case of spherically shaped micelles in the first micelle concentration range transforming to hemicapped rod-like micelles at the second CMC. Results shown in Figure 4 and Eq. [6] are in excellent agreement with the prediction. Thus, it can be suggested that in the first micelle concentration range, the shape of the micelles remains more or less invariant and only the number of micelles increases with increasing SDS concentrations. Thus, the phase transition from sphere-shaped

to hemicapped rod-like micelles occurs at the second CMC. Length of the hemicapped rod-like micelles increases with increasing SDS concentrations.

Figure 6 shows the plot of relative intensities of ANS (0.5mM) as a function of sodium laurate concentration. Sharp breaks occur at 26mM and 70mM. 26mM corresponds to the first CMC of sodium laurate. In this case fluorescence intensity slope ratio between first and second micelle concentration is 1.3.

Figure 7 presents the relative fluorescence intensity plot of ANS (1mM) as a function of SLES. Sharp breaks occur at 1.5mM and 30mM. The fluorescence intensity slope ratio between first and second micelle concentration is 1.2. These values (1.3 and 1.2) differ from the ratio of 1.5. Aqueous SDS solution exists as sphere shaped micelle in the first micelle concentration. But most detergents exist as ellipsoid shaped micelle in the first micelle concentration. Also, a phase transition from ellipsoidal to hemicapped rod-like micelle occurs at second CMC. (Figure 8).

In the first micelle concentration, we have

$$\frac{x^2}{a^2} + \frac{y^2}{b^2} = 1 \qquad ; \text{ equation of ellipse}$$

$$V_1 = 2\pi \int_0^a y^2\, dx = \frac{4}{3}\pi ab^2$$

$$S_1 = (\frac{4}{3}\pi b^2 + \frac{8}{3}\pi ab)\, n_1$$

$$m = \frac{4}{3}\pi ab^2\, n_1\, \rho$$

$$(dS_1/dm)_{a,b} = \frac{1}{\rho}(\frac{1}{a} + \frac{2}{b}) \qquad [1]$$

where V_1, S_1 and m stand for total volume, surface area and mass of micelle in the first micelle concentration, respectively.

Similarly, in the second micelle concentration,

$$S_2 = (\frac{4}{3}\pi b^2 + \frac{8}{3}\pi ab + 2\pi b \cdot 1)\, n_2$$

$$m = (\frac{4}{3}\pi ab^2 + \pi b^2 1)\, n_2\, \rho$$

$$(dS_2/dm)_{a,b,n_2} = 2/b\rho \qquad [2]$$

$$\frac{(dS_1/dm)_{a,b}}{(dS_2/dm)_{a,b,n_2}} = \frac{b}{2a} + 1 \qquad [3]$$

From Figure 6,

$$\frac{dI_1/dC}{dI_2/dC} = 1.3 \qquad [4]$$

From [3] and [4]

$$\frac{b}{2a} + 1 = 1.3 \qquad \therefore\ a : b = 5 : 3$$

The axial ratio of sodium laurate ellipsoid micelle in the first micelle concentration is 5:3.

From Figure 7,

$$\frac{dI_1/dC}{dI_2/dC} = 1.2$$

$$\frac{b}{2a} + 1 = 1.2 \qquad \therefore\ a : b = 5 : 2$$

The axial ratio of SLES ellipsoid micelle in the first micelle concentration is 5:2.

The general formula, $\frac{dI_2/dC}{dI_2/dC} = \frac{b}{2a} + 1$, is suggested for the axial ratio of ellipsoid shaped micelle.

The phase transition from spherically shaped micelles to hemicapped rod-like micelles is facilitated by electrolytes.

Figure 9 shows the relative fluorescence intensities of ANS (0.32mM) in 8mM SDS solutins as a function of NaCl concentrations. Results shown in this figure suggest that the ANS fluorescence increases rapidly with NaCl, as CMC is lowered and micelle formation is facilitated by electrolytes.

Figure 10 plots mole ratios of solubilized benzene in 5mM SDS solution as a function of NaCl concentration. The detergent in 5mM SDS solution exists as monomers and has no solubilizing properties. However, its solubilizing power increases rapidly as micelle formation is facilitated by electrolytes, consistent with the trend shown in Figure 9.

Figure 11 shows the F_2/F_1 plot of pyrene (0.3mM) is 40mM SDS solution as a function of NaCl concentration. The values of F_2/F_1 increase with increasing concentrations of the electrolytes. This suggests that sphere-shaped micelles in 40mM SDS solution are transformed to hemicapped rod-like micelles and the length of the latter continues to increase with increasing electrolyte concentrations.

Figure 12 presents mole ratios of solubilized benzene in 40mM SDS solutin as a function of NaCl concentrations. The maximum additive concentration of benzene in 40mM SDS solution increases rapidly as hemicapped rod-like micelles grow in the presence of electrolyte. Apparently, the CMC is

lowered and the amount of detergent participating in the micelle formation increases in the presence of electrolyte. We find that the solubilizing power of hemicapped rod-like micelles for benzene is superior to that of sphere-like micelles.

REFERENCES

1. Birdi, K.S. Colloid Polym. Sci., *252*, 551 (1974).
2. Cowichene, W.L. J. Phys. Chem., *68*, 1870 (1964).
3. Götz, K.G. and Heckmann, K. J. Colloid Sci., *13*, 266 (1958).
4. Ekwall, P., Mandell, L. and Solyom, P.J. Colloid Interface Sci., *35*, 519 (1971).
5. Rohde, A. and Sackmann, E.J. Colloid Interface Sci., 70, 494 (1979).
6. Ikeda, S., Ozeki, S. and Tsunoda, M.A. J. Colloid Interface Sci., *73*, 27 1980).
7. Reiss-Husson, F. and Luzzati, V. J. Phys. Chem., *68*, 3504 (1964).
8. Povkh, I.L. Kucher, R.V., Shevhcuk, I.A., Serdyuk, A.I., V Vashun, Z.M. and L'vov, V. zh. Prik. Him., *51*, 1045 (1978).
9. Kodama, M. J. Sci. Hiroshima Univ., Ser. A *37*, 53 (1973).
10. Turro, N.J. and Yekta, A.J. Am. Chem. Soc., *100*, 5951 (1978).
11. Turro, N.J. Modern Molecular Photochemistry, W.A. Benjamin, Menlo Park, CA, p. 141, 1978.
12. Kalyanasundaram, K., Gratzel, M., and Thomas, J.K. J. Am. Chem. So., *97*, 3915 (1975).
13. Masaji, M. Bull. Chem. Soc. Jpn., *45*, 428 (1972).
14. Granath, K. Acta Chem. Scand., 7, 297 (1953).
15. Mukerjee, P. and Mysels, K.J. Nat. Standard Ref. Data Service, National Bureau of Standards, No., *36*, 15 (1971).
16. Rehfeld, S.J. J. Phys. Chem., *74*, 117 (1970).
17. Kim, J. S., Kim, C.K., Lee, K.M., and Song, P.S., J. Colloid Interface Sci., *80*, 294 (1981).

FIGURE . 1

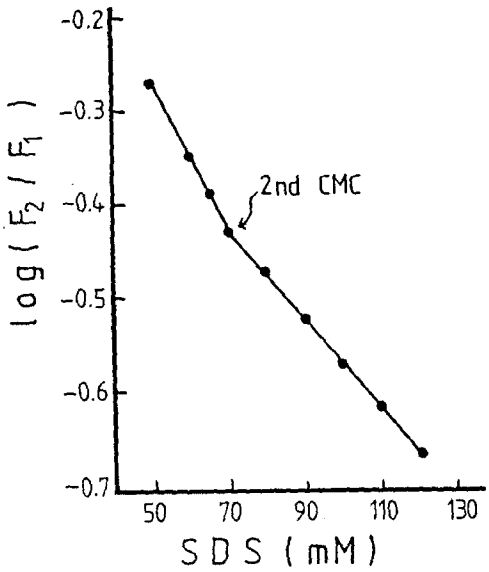

FIGURE . 2

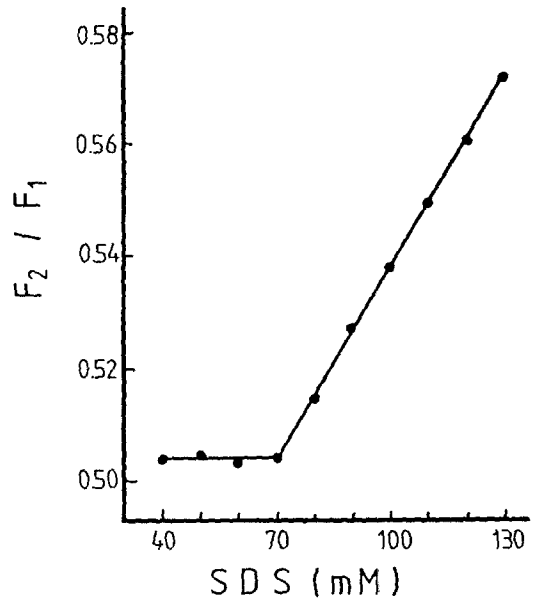

FIGURE . 3

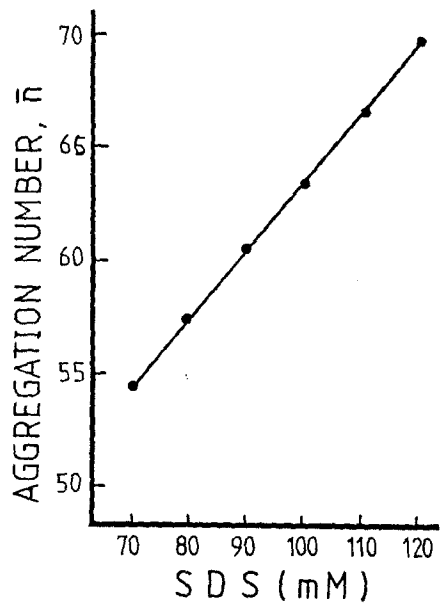

FIGURE 4

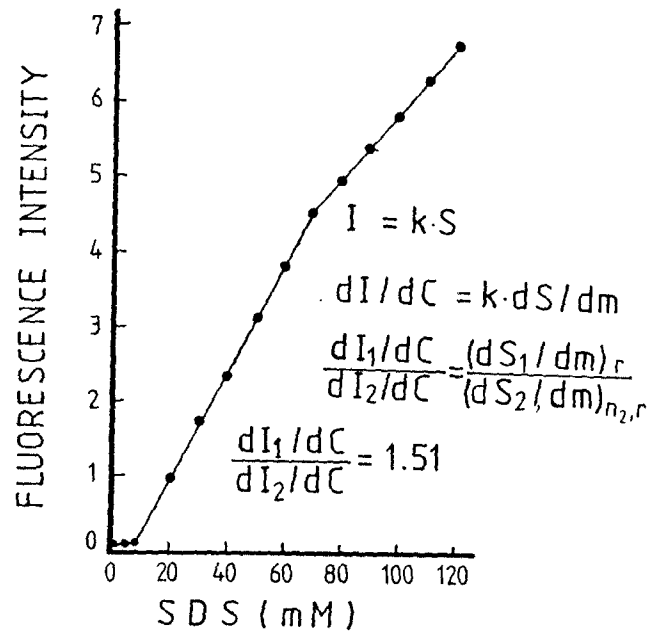

FIGURE 5

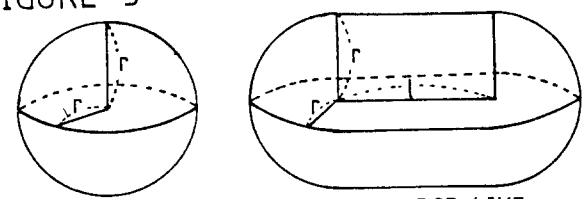

SPHERICAL MICELLE

HEMICAPPED ROD-LIKE MICELLE

In the 1st micelle concentration,

$S_1 = 4\pi r^2 n_1$, $m = \frac{4}{3}\pi r^3 \rho n_1$

In the 2nd micelle concentration,

$S_2 = (4\pi r^2 + 2\pi r l) n_2$,

$m = (\frac{4}{3}\pi r^2 + \pi r^2 l)\rho n_2$

$$\frac{(dS_1/dm)_r}{(dS_2/dm)_{n_2,r}} = 1.5$$

From Figure 4 ,

$$\frac{dI_1/dC}{dI_2/dC} = 1.51$$

FIGURE 6

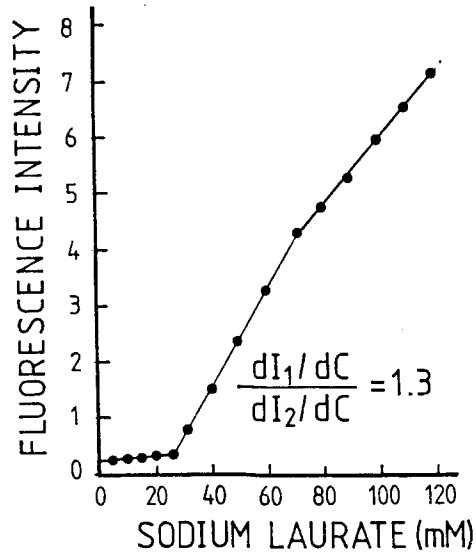

FIGURE 7

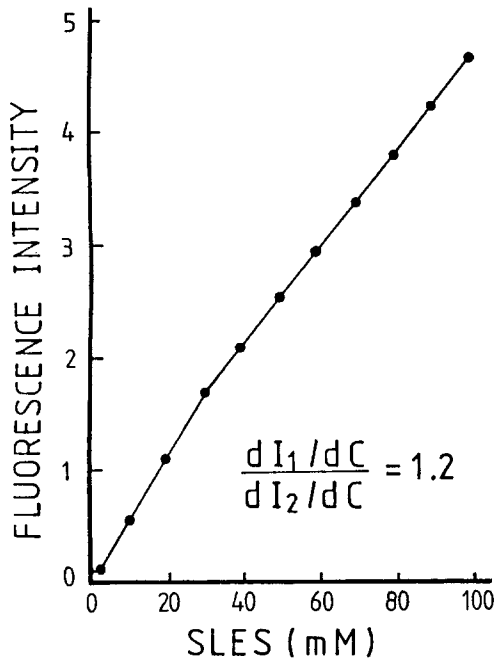

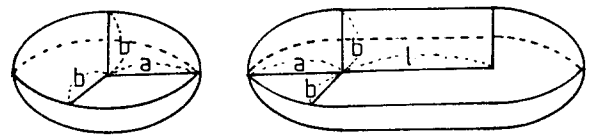

ELLIPSOID MICELLE

HEMICAPPED ROD-LIKE MICELLE

In the 1st micelle concentration,

$S_1 = (\frac{4}{3}\pi b^2 + \frac{8}{3}\pi ab) n_1$, $m = \frac{4}{3}\pi ab^2 n_1 \rho$

In the 2nd micelle concentration,

$S_2 = (\frac{4}{3}\pi b^2 + \frac{8}{3}\pi ab + 2\pi bl) n_2$

$m = (\frac{4}{3}\pi ab^2 + \pi b^2 l) n_2 \rho$

$$\frac{(dS_1/dm)_{a,b}}{(dS_2/dm)_{a,b,n_2}} = \frac{b}{2a} + 1$$

From Figure 6,

$$\frac{dI_1/dC}{dI_2/dC} = 1.3 \quad \therefore a:b = 5:3$$

From Figure 7,

$$\frac{dI_1/dC}{dI_2/dC} = 1.2 \quad \therefore a:b = 5:2$$

FIGURE . 9

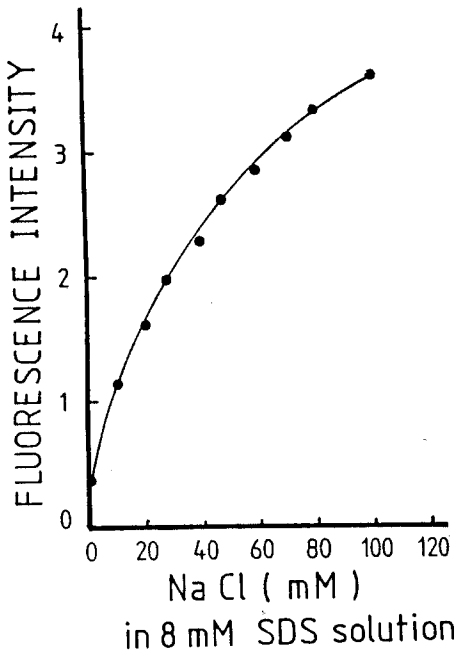

FIGURE . 10.

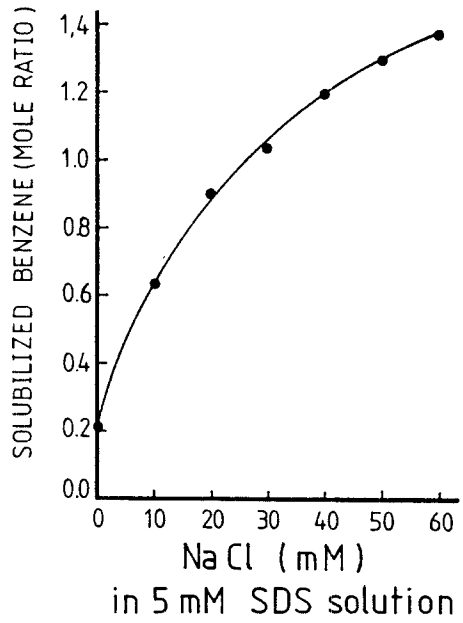

FIGURE 11

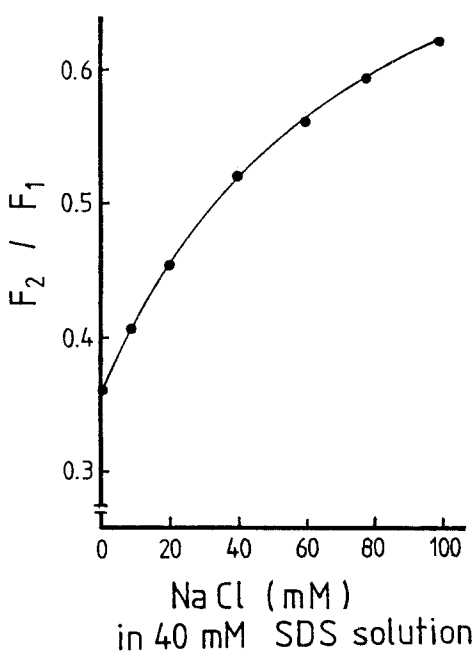

FIGURE 12